arXiv:astro-ph/0504336v1 14 Apr 2005

Accepted for Publication in the Astrophysical Journal

Spitzer Detection of PAH and Silicate Dust Features in the Mid-Infrared Spectra of $z \sim 2$ Ultraluminous Infrared Galaxies

Lin Yan

R. Chary, L. Armus, H. Teplitz, G. Helou, D. Frayer, D. Fadda, J. Surace, P. Choi

Spitzer Science Center, California Institute of Technology, MS 220-6, Pasadena, CA 91125

lyan@ipac.caltech.edu

ABSTRACT

We report the initial results from a Spitzer GO-1 program to obtain low resolution, mid-infrared spectra of infrared luminous galaxies at $z \sim 1-2$. This paper presents the spectra of eight sources observed with the *Spitzer* InfraRed Spectrograph (IRS). Of the eight spectra, six have mid-IR spectral features, either emission from Polycyclic Aromatic Hydrocarbon (PAH) or silicate absorption. Based on these mid-IR features, the inferred six redshifts are in the range of $1.8-2.6$. The remaining two spectra detect only strong continua, thus do not yield redshift information. Strong, multiple PAH emission features are detected in two sources, and weak PAH emission in another two. These data provide direct evidence that PAH molecules are present and directly observable in ULIRGs at $z \sim 2$.

The six sources with measured redshifts are dusty, infrared luminous galaxies at $z \sim 2$ with estimated $L_{bol} \sim 10^{13} L_{\odot}$. Of the eight sources, two appear starburst dominated; two with only power law continua are probably type I QSOs; and the remaining four are likely composite systems containing a buried AGN and a starburst component. Since half of our sample are optically faint sources with $R \geq 25.5$ mag (Vega), our results demonstrate the potential of using mid-infrared spectroscopy, especially the Aromatic and silicate features produced by dust grains to directly probe optically faint and infrared luminous populations at high redshift.

Subject headings: galaxies: infrared luminous – galaxies: starburst – galaxies: high-redshifts – galaxies: evolution

1. Introduction

Numerous studies over the past decade have found that star-forming galaxies have undergone strong evolution in their luminosity and number density since redshift of $1-2$, and that luminous and ultraluminous infrared galaxies play a critical role in this evolution. The peak of the far-infrared background detected by *COBE* is at $\sim 200\mu$m, with energy comparable to the optical/UV background (Puget et al. 1996; Fixsen et al. 1998). This implies that $\sim$50% of the integrated rest-frame optical/UV emission in the universe has to be thermally reprocessed by dust and radiated at the mid to far-infrared. Deep ISO 15μm number counts, and more recently, *Spitzer* 24μm number counts, suggest a large excess of mid-IR sources compared to the predictions by nonevolving models (Marleau et al. 2004; Papovich et al. 2004; Chary et al. 2004; Gruppioni et al. 2002). Particularly, the *Spitzer* 24μm number counts imply that a significant population of sources with flux densities on the order of 100μJy are likely infrared luminous galaxies at $z \sim 1-3$, previously undetected in the ISO data. Furthermore, the strong evolution of infrared luminous galaxies at $z \lesssim 1$ was directly characterized by the infrared luminosity functions from studies of ISO 15μm sources with optical redshifts (Elbaz et al. 1999; Serjeant et al. 2000; Franceschini et al. 2002; Elbaz et al. 2002), In addition, optical spectroscopy of optically faint, radio-selected, $S_{850} > 6$ mJy submillimeter galaxies has found that these sources are at a median redshift of 2.3 (Chapman et al. 2005, 2003). Their inferred volume density, $\sim 1.3 \times 10^{-5}$Mpc^{-3} at $L_{IR} \geq 4 \times 10^{12} L_{\odot}$, is roughly two to three orders of magnitude higher in comparison with the local density of IRAS ultraluminous galaxies at the similar luminosity limit (Soifer et al. 1987).

Although ISO and sub-mm observations have revealed many tantalizing facets of the dusty universe at $z \sim 1-3$, the successful launch of *Spitzer*, with its combined fast photometric mapping and spectroscopic capabilities, has made it possible to discover and characterize large numbers of dusty, infrared luminous galaxies at cosmologically interesting redshifts. Of critical significance is that the mid-IR spectroscopic properties of infrared luminous galaxies at $z > 0.5$ are virtually unknown. The mid-IR spectra of starburst galaxies and most ULIRGs are dominated by the emission and absorption features of dust grains. While the shape of the mid-IR continuum and its brightness relative to the far-infrared constrain the amounts of hot and cold dust, the strong PAH emission features at 6.2, 7.7, 8.6, 11.3, and 12.7μm and silicate absorption (centered at 9.7 and 18μm) provide both an indication of the type of source heating the dust (since PAH's are easily destroyed by UV photons and x-rays from an AGN) and redshift estimates for sources that are completely obscured at shorter wavelengths (Genzel & Cesarsky 2000; Draine 2003; Laurent et al. 2000; Tran et al. 2001; Rigopoulou et al. 1999; Voit 1992). With the sensitivity and wavelength coverage of the InfraRed Spectrograph (Houck et al. 2004, IRS;) on *Spitzer*, it is now possible to obtain the

mid-IR spectral diagnostics of dusty galaxies out to $z \sim 3$.

In this paper, we report initial results of a GO-1 program to obtain low resolution, mid-infrared spectra of a sample of 52 galaxies in the *Spitzer* First Look Survey (FLS)[1] over an area of 3.7deg^2. Our targets were potential high redshift candidates, selected based on the color criteria described in detail in §2. Eight sources in our target sample were observed between August 27 to September 6, 2004, while the remainder of the full sample has been scheduled for 2005. In this paper, we report the first results from the analyses of these eight targets. These eight sources have 24μm fluxes and mid-IR colors representative of the full sample, and provide an initial look at the data we expect to obtain for the complete sample. Since very few mid-IR spectra of galaxies with $z > 1$ have been published, and the lifetime of Spitzer is short, these initial results are valuable for planning future IRS observations of high-redshift, luminous infrared galaxies. The paper is organized as follows. §2 describes the our target selection and the IRS observation design in detail; §3 discusses the imaging reduction and 1D spectral extraction procedures we used in this dataset; §4 presents the results and we discuss the implications of our findings in §5. Throughout the paper, we adopted the cosmology of $\Omega_m = 0.27, \Omega_\Lambda = 0.73$ and $H_0 = 71\,\mathrm{km\,s^{-1}\,Mpc^{-1}}$.

2. Target Selection and Observations

Our *Spitzer* GO-1 program was designed to obtain mid-infrared spectra of a sample of 24μm sources, selected to be starburst candidates at $z \gtrsim 1-2$ based on their mid-IR colors. The *Spitzer* data used for our target selection are the 24 and 8μm catalogs from the FLS main survey region (Fadda et al. 2005; Marleau et al. 2004; Lacy et al. 2005). In order to obtain good quality IRS spectra in reasonably short integration times, we required all spectroscopic targets to be brighter than 0.9mJy at 24μm. We applied additional color constraints in order to select potential starburst galaxies at $z > 1$. This is based on 24/8 and 24/0.7 micron colors. Here we define $R(24,8) \equiv \log_{10}(\nu f_\nu(24\mu m)/\nu f_\nu(8\mu m))$, and $R(24,0.7) \equiv \log_{10}(\nu f_\nu(24\mu m)/\nu f_\nu(0.7\mu m))$. The criteria used to select the IRS targets are $R(24,8) \geq 0.5$ and $R(24,0.7) \geq 1.0$. These color cuts are determined by comparing the observed 24/8 and 24/0.7 μm color distributions of *all* 24μm sources over the FLS region with the computed color tracks as a function of redshift using a set of known mid-IR spectral templates. The detailed discussion on the mid-IR color distributions in the FLS has been published in Yan et al. (2004). The $R(24,0.7) \geq 1.0$ condition is a crude redshift selection, and the $R(24,8) \geq 0.5$ cutoff selects sources with very steep, red continua, as seen

[1]For details of the FLS observation plan and the data release, see http://ssc.spitzer.caltech.edu/fls.

in many local starbursts and ULIRGs (Armus et al. 2004; Genzel et al. 1998; Lutz et al. 1998; Rigopoulou et al. 1999). In §5, we will discuss how well our selection criteria work with respect to our observations.

Over the 3.7deg^2 region, a total of 59 sources meet the 24μm flux and the color cuts. Due to the limited number of hours available to our program, we targeted 52, chosen randomly from the total 59 sources. For all of the targets, we obtain low resolution ($\frac{\lambda}{\Delta\lambda} = 64 - 128$) spectra in Long-low module of the IRS (LL, 14 – 40μm). For a few sources with the IRAC 8μm fluxes greater than 150μJy, we also obtained 1st order, Short-low spectra (SL, 7.5–14μm). Table 1 lists the positions, the broad band 24μm, 8μm and R-band fluxes, and the exposure times for these eight sources. In all of the observations, we used nearby bright stars as peak-up to accurately center the slit on the science targets. The IRS slit width is 3.7$''$ for the SL and 10.7$''$ for the LL. Our targets are all unresolved, point sources with the full-width-half-maximum (FWHM) of $\sim 2''$ and $\sim 6''$ in the 8 and 24μm images respectively. Thus, in our IRS observations there should be neglible light loss due to the finite IRS slit width.

3. Data Reduction and Analyses

3.1. Imaging Processing

The raw spectral data are first processed by the IRS pipeline (S11.0.2 version) at the Spitzer Science Center (SSC). The processing steps taken by the IRS pipeline include ramp fitting, dark sky subtraction, droop correction, linearity correction, flat fielding, and wavelength and flux calibration. For our SL data, stray light correction is not necessary because the peak-up images do not have any sources bright enough to have significant stray light contaminations in the SL spectra. We therefore used the uncorrected output from the SSC pipeline.

Starting with the 2-dimensional (2D) Basic Calibrated Data (BCD) produced by the IRS pipeline, we performed additional processing, including background subtraction and making new bad pixel mask for the coadded image at each nod position. The background subtraction was tested with three different methods: (1) The subtraction of a "supersky", constructed by median combining all of the available 2D images, excluding the images at the same order and the same nod position. This supersky is scaled and then subtracted from the individual exposure before summing up all exposures at each nod position, (2) By differencing the exposures at two nod positions along the slit, then summing up all the exposures at the same nod position, (3) The subtraction of a supersky constructed only from

the exposures within a single AOR. The supersky methods (1 & 3) improve the background signal-to-noise ratio by ∼10-20%. However, for some fields, when the mean background levels are significantly different from the supersky, the number of "warm pixels" can be higher than using the difference of the nod positions. In these cases, we simply take the difference of the two nod positions. In all cases, we chose the subtraction method that gives the best signal-to-noise ratio as well as the fewest number of residual bad pixels.

After the background subtraction, we compare the 2D spectra of the same target at the two nod positions and remove any bad pixels within the spectral extraction aperture by visual examination. Usually, there are less than 10 pixels which need to be masked manually in addition to the bad pixel masks. These bad pixels are not considered in the subsequent, 1D extracted spectra, and do not contribute to the final average of the spectra from the two nod positions.

3.2. Spectral Extraction

As described in §2, spectra were taken in two nod positions for each IRS slit. One-dimensional (1D) spectra were extracted, then averaged to produce the final 1D spectrum for each module. The spectral extraction is done using the SSC software SPICE v1.3[2]. SPICE is a Java based tool which allows the user to interactively display and extract IRS spectra. The spectral centroiding and extraction aperture can be adjusted to maximize the S/N ratio. For our data, we used an extraction aperture, whose width is 1 or 2 pixels narrower than the default PSF size in SPICE, and the shape of the extraction aperture simply follows the PSF size as a function of wavelength. This method minimizes the uncertainties due to the background, and maximizes the S/N ratios for faint spectra. We used the simple method of summing up the light within the extraction aperture and did not use optimal extraction technique for our data. The version of all of the calibration files used by SPICE is consistent with the IRS pipeline version S11.0.2. The flux scales of the final, averaged SL and LL spectra were set by using the IRAC 8μm and MIPS 24μm broad band fluxes. The accuracy of our flux calibration is thus primarily determined by the IRAC 8μm and MIPS 24μm calibration errors, roughly (5-10)% (see the *Spitzer* Observers Manual; also Reach et al. in prep).

[2]see the ssc webpage http://ssc.spitzer.caltech.edu/postbcd/spice.html for the description of the software and the public release status.

4. Results

4.1. Spectra and Redshift Measurements

Figure 1a,b,c,d show the 1D spectra of the eight sources observed by the IRS. In Figure 1, the color coded lines represent the 1D spectra in the original resolution, with the red segment for the IRS LL 1st order, the blue for the LL 2nd order, and the green for the SL 1st order. To aid the identification of PAH emission features, we smoothed our observed 1D spectra by roughly 5-7 pixels. The smoothed spectra are shown by the black lines, and are shifted by an arbitary amount in the Y-axis for viewing clarity. The smoothing kernel is a boxcar, and roughly $5-7$ pixels wide. The size of the smoothing kernel is chosen so that at the rest-frame wavelength it is similar to the the rest-frame FWHM of the 7.7μm PAH emission in UGC 5101 (Armus et al. 2004). Strong, multiple PAH emission features (6.2,7.7,8.6 and 11.2μm) are detected in two sources, IRS9 and IRS2, and weak PAH emission (7.7μm and 6.2μm or 8.6μm) in additional two (IRS6 and IRS11). A broad absorption trough, roughly centered at the observed wavelength of 27-36μm, is also detected in six out of eight spectra. We associate this broad feature with redshifted silicate absorption at a central rest-frame wavelength of 9.7μm. Based on these emission and absorption features, the inferred redshifts are in the range of $1.8 < z < 2.6$ for these six sources. The remaining two spectra (Figure 1d) have well detected continua, but no other identifiable spectral features. The redshifts for these two sources are unknown.

For the six sources with either PAH emission and/or silicate absorption at the rest-frame 9.7μm, we measure their redshifts using the following procedures. Two of our sources have only broad silicate absorption troughs, thus, their redshift measurements have large errors, on the order of 0.1-0.2. In the remaining four sources, we have multiple spectral features, both PAH emission and silicate absorption. PAH features are generally sharper than silicate absorption, thus give more accurate measurements of redshifts. In each of these cases, the final redshift is determined by the combined z measurements from the multiple features. Specifically, for each PAH feature, the redshift $(1+z)_i$ is derived as $\lambda_{obs}(i)/\lambda_{rest}(i)$. Here i indicates one of the PAH features, and its rest-frame wavelength is measured from the spectra of local starburst galaxies taken with the IRS in the same slit and resolution. The local reference spectra were NGC7714 and UGC5101 (Brandl et al. 2004; Armus et al. 2004). The final redshift is the average value of z_i, and the error is computed as $\sigma = \frac{\sqrt{\sum_i (z_i - <z>)^2}}{\sqrt{n-1}}$. The redshift discrepencies between different PAH features reflect the contributions from the wavelength measurement error in determining the centroid of PAH feature and the systematic errors in the IRS wavelength calibration. Sharper PAH emission features will have smaller measurement errors in the wavelength centroids. The redshifts for the six sources are in the

range of 1.8-2.6. The redshift errors for IRS2 and IRS9 are smaller, since both have PAH emission lines at 6.2, 7.7, 8.6 and 11.2μm. IRS9 has four strong PAH features. Its 6.2 and 11.2μm features are narrow and used for the final redshift determination. The spectrum for IRS11 is peculiar. Its absorption line at 9.7μm is saturated with a flattened bottom. This is reflected in the large uncertainty, 0.2, for its redshift.

An alternative way of determining the redshift is to fit the observed spectra using a set of mid-infrared spectral templates of local galaxies with prominent PAH and silicate features (template cross-correlation method). We found that the redshifts measured from these two methods are consistent. The limitation in the template cross-correlation method is that it has to assume some templates and it is difficult to determine what local template spectra are representative of high redshift spectra. For this paper, we are limited to a few, high quality spectra which have been published. We have used the interpolated model templates from Chary & Elbaz (2001), as well as the published IRS spectra of UGC 5101, Mrk1014, IRAS F00183-7111 and NGC7714 (Armus et al. 2004; Spoon et al. 2004; Brandl et al. 2004). The strongest signal for determining redshift using the template fitting method comes from the silicate absorption feature. For this paper, we choose to use redshifts measured from PAH and silicate features. Table 2 presents the redshifts and the errors for the six targets.

4.2. PAH Emission and Silicate Absorption Features

Multiple, strong PAH emission features are detected in two sources and weak PAH emission in additional two. Table 2 lists the PAH flux and its S/N for each feature. The flux is measured by fitting a gaussian profile with continuum subtracted, and a linear continuum computed over roughly a wavelength range of $\lambda_0 \pm 1.5\mu m$ (λ_0 being the fitted PAH feature). Given our low S/N spectra, we have adopted this simple approach to measure the continuum and the line flux. The 1σ noise for each PAH feature is computed as $1\sigma = rms \times \sqrt{n} \times \Delta\lambda$, where rms is the noise per pixel measured from the continuum near the emission line, n is the FWHM of the emission line in pixel, and $\Delta\lambda$ is the size of the pixel in μm/pixel. The significance of the detection (S/N) is computed as $S/N = flux(PAH)/1\sigma$. The rms is measured from the original spectrum and the feature profile fitting is done with the smoothed spectrum. As shown in Table 2, the S/N ratio for each individual PAH feature is geater than 3 for IRS2 and IRS9, and in the range of $1.5 - 2.5$ for IRS6 and IRS9. Although individual S/N ratio seems to be small, the final redshift measurement is much more reliable when the identified, multiple features are consistent.

One pecularity about the IRS9 spectrum is its unusually strong 11.2μm line, in comparison with UGC5101, F00183-7111 and NGC7714 (Brandl et al. 2004; Armus et al. 2004;

Spoon et al. 2004). The relative line luminosity between 6.2 and 11.2μm is 0.75 for IRS9. One study in local HII regions (Vermeij & van der Hulst 2002) seems to suggest that this ratio less than 1 are mostly in low metallicity objects. In addition, the theoretical models of PAH emission (Draine & Li 2001) show that luminosity ratio of 11.2-to-7.7μm features is closely linked to ionization state of PAH, and the high ratio is indicative of presence of a large amount of neutral PAH, with ISM similar to photo-disassociate-region (PDR).

The strength of silicate absorption is an excellent indicator of dust extinction at the mid-infrared. Precise measurement of the absorption strength sometimes can be difficult when the feature is not very strong and the continuum is affected by strong PAH emission at the both side of the absorption trough. Of the six targets with redshifts, at least four have strong silicate absorption. In the other two sources, IRS9 and IRS11, the absorption due to silicate material is probably present, but the estimate of the depth of the absorption is largely uncertain. This is mainly due to the poor determination of the continuum level using the low S/N spectra covering a fairly narrow wavelength region.

Although comprehensive modeling of our mid-IR spectra is beyond the scope of this paper, we can use the following methods to provide a simple estimate of the dust obscuration in our sources. The depth of the absorption feature can be used as an indication of the obscuration. The opacity at the bottom of the silicate absorption trough is estimated as $\tau_{9.7\mu m} = \ln(S_c/S_{min})$, where S_c and S_{min} are the flux densities at the center of the trough without and with absorption respectively. The continuum is measured using clean continuum location at rest-frame 7 and 14μm. S_{min} is taken as the minimum of the flux density at the bottom of the absorption trough. Table 2 lists $\tau_{9.7\mu m}$ values for the six sources we detect the silicate absorption. The amount of dust obscuration is highly uncertain in IRS11. Its spectrum shows that the absorption minimum is flattening out to zero, suggesting a large amount of dust along the line-of-sight. However, the level continuum for this source could also be low, thus the inferred absorption strength would be small. It requires a better S/N ratio spectrum to draw more definitive conclusion on its dust obscuration for this object. From $\tau_{9.7\mu m}$ listed in Table 2, the implied extinction at the visible wavelength is large, if we assume $A_V/\tau_{9.7\mu} = 18.5 \pm 2.0$ (Draine 2003). The estimated lower limits on A_V is $\sim 14 - 56$ magnitudes, which is comparable to that of local ULIRGs.

Another method would be to use the absorption coefficients computed by Li & Draine (Li & Draine 2001), based on a simple cold screen model. The computed spectra, $I_\nu/I_\nu(cont) = e^{-N*C_{ext}}$, are used to fit the observed spectra between in the rest-frame $6 - 12\mu$m. The estimated column density is in the range of $(2 - 10) \times 10^{22}\mathrm{cm}^{-2}$. We should point out that the uncertainties in the quantative analyses of silicate absorption feature and the dust extinction are mostly from determination of continuum and unknown geometric distribution

of dust. While both estimates of the extinction towards the line of sight to the nuclei are valid, major uncertainties remain concerning the distribution of the dust, the dust-to-gas ratio, the metallicity and the proper level of the continuum. Therefore, the derived values should be treated as rather uncertain estimates of the lower limit of extinction along the line of sight to the nuclei of these high-redshift galaxies.

4.3. Bolometric luminosity

While our IRS spectra covering the rest-frame 5-15μm do provide constraints on the slopes of the mid-IR SEDs, the far-infrared emission, which dominates the bolometric luminosity, remains unconstrained for most of our sample, except IRS9. For IRS9, we have a MIPS 10σ detection at 70μm with the flux of 42mJy. At 160μm, we have only a 3σ upper limit of 150mJy. IRS9 is also detected at 1.2mm with 6σ of 2.5mJy with MAMBO (Lutz et al. 2005). Combining all of the data together, we estimate that L_{IR} for IRS9 is $1.8 \times 10^{13} L_{\odot}$. The uncertainty for IRS9 is probably witin a factor of 2-3. For the remaining five sources with redshifts, the crude estimates of their bolometric luminosities were done using the template fitting method. As templates, we used the IRS spectra of UGC5101, Mrk1014, IRAS F00183-7111 and NGC7714 (Brandl et al. 2004; Armus et al. 2004; Spoon et al. 2004).

The derived bolometric luminosities are in the range between $(0.5 - 5) \times 10^{13} L_{\odot}$. These luminosities are likely uncertain to factors of $5 - 10$ because the selection of the best-fit, rest-frame mid-infrared spectrum from a limited number of templates does not ensure an accurate estimate of the bolometric luminosity, especially the cold dust component. However, since the templates include pure starbursts, composite sources, and pure AGN, they likely provide a fair representation in bolometric luminosity, energetic type and degree of dust obscuration, of the sources in our sample. IRAS F00183-7111 is very luminous, highly obscured source, UGC 5101 has a powerful starburst and a buried AGN, Mrk 1014 is a type-1 dusty QSO, and NGC 7714 is a bright, nearby starburst (not a ULIRG). Both Mrk 1014 and NGC 7714 have very little extinction along the line of sight to their nuclei (as evidenced by the lack of silicate absorption in their IRS spectra). With these uncertainties in mind, our derived luminosities suggest that the observed galaxies are as luminous, and likely much more luminous, than typical low-redshift ULIRGs. More importantly, our sources with PAH emission features are a factor of (5-10) more luminous than starburst dominated ULIRGs in the local Universe.

5. Discussions

5.1. The Nature of our sources

With redshift information, we compute PAH luminosities and estimate their contributions to the bolometric infrared luminosities. Table 3 lists the PAH-to-bolometric luminosity ratios and the rest-frame equivalent widths, including the data for the local benchmarks. The $L_{7.7\mu m}/L_{IR}$ is 10^{-3} and 2.2×10^{-3} for IRS2 and IRS9 respectively. These values are similar to UGC5101, a highly obscured and starburst dominant system. And they are much higher than those of Mrk1014 (type-I, IR loud QSO) and F00183-7111 (a highly obscured composite ULIRG). The rest-frame equivalent widths at 6.2 and 7.7μm are comparable to those of UGC5101 in IRS9. In IRS2 the equivalent widths are smaller than in UGC 5101 bu about a factor of three. The IRS spectra of IRS9 and to a lesser extent, IRS2, both indicate a dominant contribution to the bolometric luminosity from a dusty starburst (as in UGC 5101). In IRS2 a buried AGN might be contributing at IRS wavelengths, decreasing the equivalent width of the PAH features by increasing the continuum from hot dust. The starburst-like nature of IRS9 is further supported by its detections at 70μm with *Spitzer* and at 1.2mm with MAMBO on IRAM 30 meter telescope.

For comparison with published ISO results on the PAH emission strength in ULIRGs, we measured the 7.7μm line-to-continuum ratio $(l/c)_{7.7\mu m}$ for IRS2 and IRS9. With two anchor points at the rest-frame 7 and 14μm, the ratios are 1 and 1.3 for IRS9 and IRS2 respectively. An $(l/c)_{7.7\mu m} \geq 1.0$ is shown by various ISO studies to imply a dominant starburst contribution to the mid-infrared flux (Genzel et al. 1998; Rigopoulou et al. 1999). Since both IRS9 and IRS2 meet this criterion, it is likely that they are starburst-like ULIRGs.

The remaining four of the six sources with redshifts have silicate absorption, but weak or no PAH emission. In IRS6 and IRS11, the S/N of individual PAH feature is only at the level of $1.5 - 2.5$. IRS1 and IRS8 have no detectable PAH emission. If we take the PAH fluxes or 1σ upper limits, and bolometric luminosities listed in Table 2, the implied 7.7μm line-to-bolometric luminosity ratios are (2, 10, 8 and 6)$\times 10^{-4}$ for IRS1, IRS6, IRS8 and IRS11 respectively. These ratios should be taken as upper limits. Compared with those of the local galaxies in Table 3, these numbers suggest that IRS1 is probably a system mostly dominanted by an obscured AGN, whereas the remaining three sources, IRS6, IRS8 and IRS11, are dusty, composite systems with both AGN and starburst contributions to their infrared luminosities.

Finally, IRS4 and IRS10 have only continua without any identifiable spectral features. Their redshifts can not be measured from the IRS spectra. Their observed IRS spectra from 8-38μm can exclude the possibilities that these two objects have *strong* PAH emission lines

at both low and high redshifts. The observed power law continua suggest that they are probably type I QSOs, with very little PAH emission at either low or high redshifts.

5.2. Sample Selection and The Nature of the Sources

Although our statistics are poor at this stage, we can assess the effectiveness at which our color criteria select for high-redshift, dusty galaxies. Primarily, we select sources with very red 24-to-8 and 24-to-0.7 micron colors. These red color cuts are chosen to target dusty, starburst galaxies at $z \geq 1$. The IRS GTO team has recently published another sample of $z \sim 2$ ULIRGs with the Spitzer mid-IR spectra (Houck et al. 2005). One of the differences between our sample and the Houck et al. sample is in the initial target selection. We utilized IRAC 8μm photometry and applied uniform flux ratio cuts in two colors, whereas the Houck et al. sample targeted only optically faint, 24μm sources. Particularly, our red 24-to-8 μm color criterion selects sources with red, mid-IR continua. Of the eight targets, $75 \pm 31\%$ have redshifts of $z > 1$. Our selection clearly works well in targeting high redshift systems, and results in a higher fraction of sources with measurable redshifts based on the mid-IR spectra than that of the Houck et al. sample. In our small sample, at least four and possibly six sources show strong silicate absorption, indicating large columns of cold dust along the line-of-sight to the nuclei. While a red, steeply rising mid-infrared continuum suggests the presence of warm dust, the detected silicate absorption indicates also the cold dust. Our result may suggest a broad correlation between red mid-IR continua and silicate absorption. Further studies with larger samples are clearly needed. Finally, our data detected, for the first time, strong multiple PAH emission features in starbursts at $z \sim 2$, and our sample seems to have a higher fraction of systems with PAH emission than the Houck et al. sample. This could be due to the differences in the sample selection functions.

Although our sample selection was designed to target specifically starburst galaxies with strong PAH emission, the fraction of such sources in our sample is rather small, $\sim 25\%$ from this small subsample. Most of our targets seem to have either undetected, or weak, PAH emission compared to low-redshift ULIRGs. This is perhaps not surprising given the luminosity of our targets, and the fact that at low redshift, there appears to be a trend toward more AGN-like mid-IR spectra at luminosities above $5x10^{12}L_{\odot}$ (Tran et al. 2001; Charmandaris et al. 2005). A similar trend is seen in $z \sim 2$ sources with the IRS selected via different color criteria (Houck et al. 2005). We should emphasize that although these extremely luminous galaxies have AGN-like mid-IR spectra with weak PAH emission, they could still have some amount of starburst components. Local examples of this type of sources are Mrk231 and IRAS F00183-7111 (Spoon et al. 2004). Although Mrk231 has weak

PAH emission, its L_x/L_{IR} ratio is much smaller than that of a typical AGN-dominant or QSO (Braito et al. 2004), indicating that starburst contributes to the bolometric infrared luminosity. Our results suggest that we need to reach fainter apparent mid-infrared flux levels to uncover larger populations of starburst-dominated sources at these redshifts with the IRS.

For comparison, the comoving number density of sub-mm detected galaxies at $< z >= 2.2$ is roughly $6 \times 10^{-6}\mathrm{Mpc}^{-3}$ for $L_{ir} \geq 4 \times 10^{12} L_{\odot}$ (Chapman et al. 2004), and the the rest-frame UV color selected galaxies have co-moving space density of $2 \times 10^{-3}\mathrm{Mpc}^{-3}$ for the Balmer break selected galaxies at $< z >= 1.77$ and $< z >= 2.32$ (Adelberger et al. 2004). Although our current sample is very small, it is illustrative to compute the co-moving number density of infrared luminous galaxies at $z \sim 2$. Of all of the 24μm sources detected over $3.7\mathrm{deg}^2$, 59 sources meet our sample selection criteria. If we assume $75 \pm 31\%$ of these 59 sources being at $z = 2.0 \pm 0.3$, the comoving number density is $n \sim 2 \times 10^{-6}\mathrm{Mpc}^{-3}$ for $z = 2$ and $L_{IR} \geq 5 \times 10^{12} L_{\odot}$. Given the large uncertainties, our estimate is probably consistent with that of sub-mm sources and is roughly 1% of the UV selected $z \sim 2$ galaxies.

6. Summary

This paper presents the mid-IR spectra of eight sources from our *Spitzer* GO-1 program, designed to investigate the spectroscopic properties of high-redshift dusty, infrared luminous galaxies. We detect mid-IR spectral features, either emission lines from PAH or silicate absorption at 9.7μm, among six out of eight targets. The inferred redshifts, based only on the mid-IR spectra, are at $1.8 - 2.6$. The remaining two sources have strong continuum but no identifiable spectral lines. The main conclusions based on these eight mid-IR spectra are as follows.

(1) Our sample selection is effective in targeting ULIRGs at high redshifts with PAH emission and/or silicate absorption. The high 24μm to R-band flux density ratio criterion filters out low redshift galaxies, while the high $24/8\mu$m ratio favors the selection of galaxies with red, steeply rising spectra. The sample yields the redshift measurement efficiency of $75 \pm 31\%$. (2) More than half of our sample (5/8) has prominent silicate absorption lines at 9.7μm, indicative of high dust obscuration in these $z \sim 2$ sources. (3) We detect multiple PAH emission features from two sources (2/8=25%). Compared to local ULIRGs, their line-to-bolometric luminosity ratios and equivalent widths suggest that they are powered by extremely luminous starbursts. These starbursts at $z \sim 2$ are a factor of (5-10) more luminous than the local starburst dominated ULIRGs. These data are the first direct evidence that aromatic features are already a significant component of the dusty galaxy spectra as early as z=2.

(4) The remaining four of the six sources with redshifts (4/8=60%) have weak or no PAH emission, and are likely composite systems having both a starburst and a buried AGN. Although the statistics thus far are small, our selection criteria appear to be good at isolating $z \sim 2$ ULIRGs with, in most cases, spectra most resembling AGN-dominated ULIRGs at low-z. However, these data also suggest that small PAH emitting dust grains are present and directly observable in up to $20-40\%$ of our ULIRGs at $z = 2$. Since the IRS integration times we have used for these data are relatively short, this bodes extremely well for the goal of directly using *Spitzer* to spectroscopically classify high-redshift luminous infrared galaxies.

We are grateful to the IRS instrument team and the IRS instrument support team at the Spitzer Science Center for their tremendous effort to make this instrument such a great success. We thank Tom Soifer for stimulating discussions on the nature of these luminous sources. Support for this work was provided by NASA through award issues by JPL/Caltech.

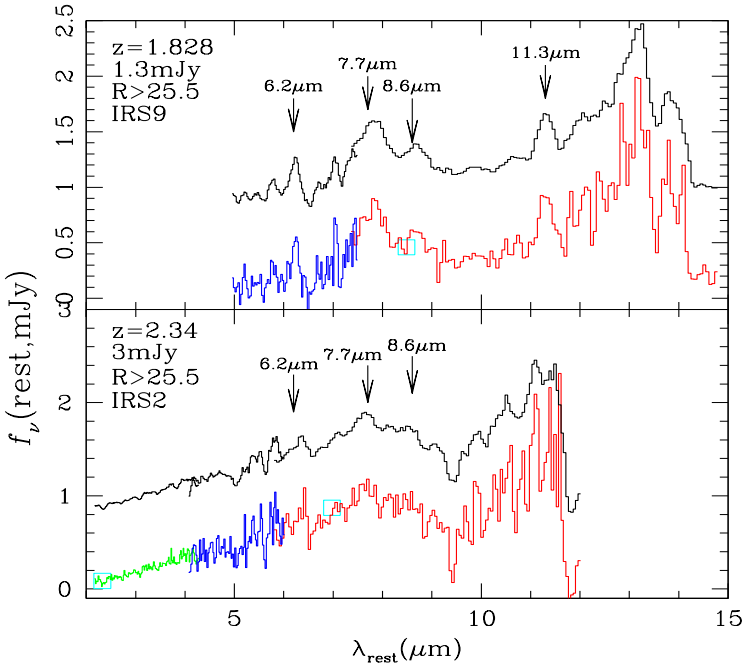

Fig. 1.— **Panel a:** Here are two spectra presented in the rest-frame flux density versus wavelength. The red, blue and green lines are the observed spectra in the original resolution, whereas the black lines are the smoothed version, and scaled with an arbitary constant in the Y-axis for viewing clarity. The red segment represents the spectrum from the IRS long-low 1st order, the blue for the 2nd order and the green is from the short-low 1st order. The open, cyan squares are the broad band rest-frame flux densities computed from the observed, broad band 8μm from IRAC and 24μm fluxes from MIPS.

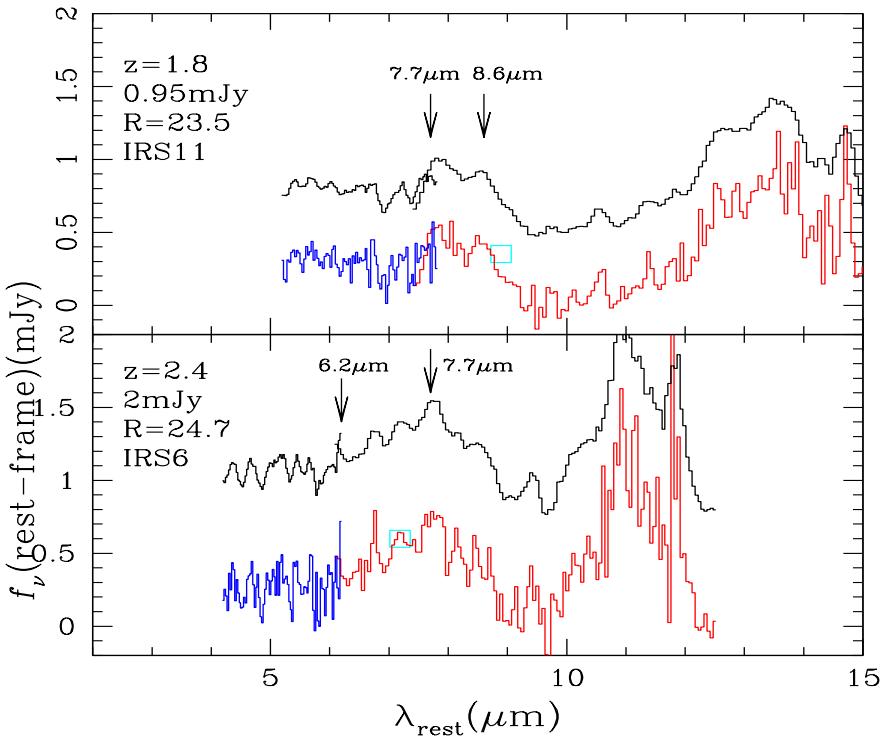

Figure 1 - Panel b: The caption is the same as in **Panel a**.

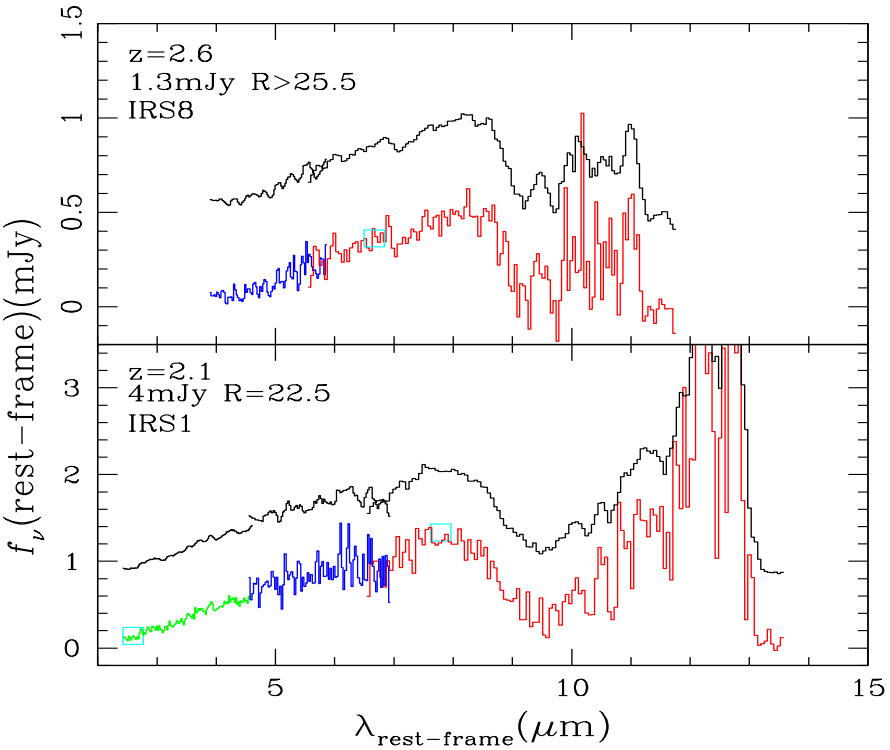

Figure 1 - Panel c: The caption is the same as in **Panel a**.

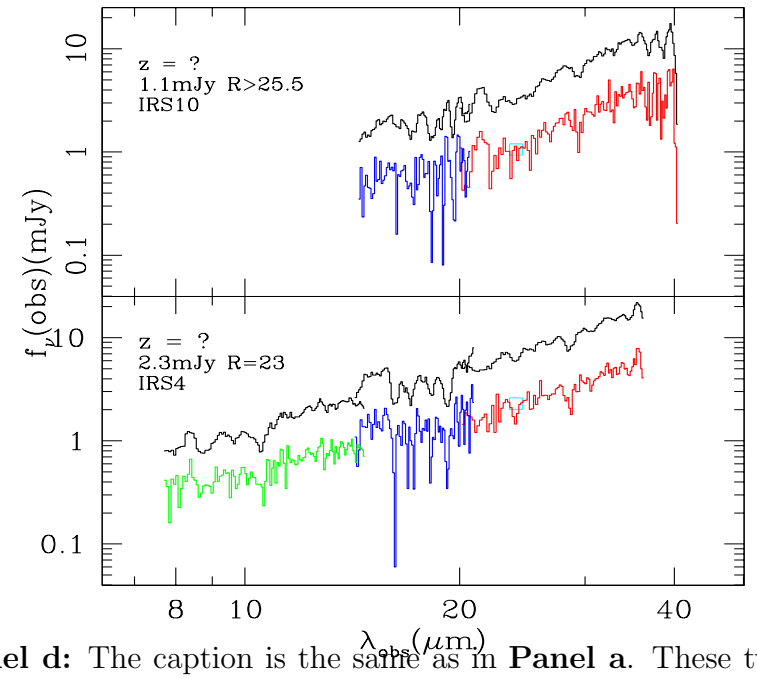

Figure 1 - Panel d: The caption is the same as in **Panel a**. These two spectra have no strong silicate absorption. IRS10 with weak PAH emission is plotted in the rest-frame, and IRS4 with no identifiable features is presented in the observed frame since the redshifts are unknown.

REFERENCES

Adelberger, K. L., Steidel, C. C., Pettini, M., Shapley, A. E., Reddy, N. A., Erb, D. K. 2004, ApJ, in press (astro-ph041065)

Alexander, D. M., et al. 2003, AJ, 125, 383

Armus, L. et al. 2004, ApJS, 154, 178

Bohlin, R. C., Savage, B. D., & Drake, J. F. 1978, ApJ, 224, 132

Brandl, B.R. et al. 2004, ApJS, 154, 188

Braito, V., et al. 2004, A&A, 420, 79

Chary, R. et al. 2004, ApJS, 154, 80

bibitem[Chary & Elbaz (2001)]chary01 Chary, R. & Elbaz, D. ApJ, 556 562

Chapman, S. C., Blain, A. W., Smail, I., & Ivison, R. J. 2005, ApJ, 622, 772

Chapman, S. C., Smail, I., Blain, A. W., & Ivison, R. J. 2004, ApJ, 614, 671

Chapman, S.;Blain,A.W.;Ivison,R.J.;Smail,I.R. 2003, Nature, 422, 695

Draine, B. T. & Li, A. 2001, ApJ, 551, 807

Draine, B. T. 2003, ARA&A, 41, 241

Elbaz et al. 1999, A&A, 351, 37

Elbaz,D.;Cesarsky, C.J.;Chanial,P.;Aussel,H.;Franceschini,A.;Fadda,D;Chary,R.R. 2002, A&A, 384, 848

Fadda, D. et al. 2005, ApJ, in prep

Fixsen,D.J.; Dwek,E.; Mather,J.C.;Bennett,C.J.;Shafer,R.A. 1998, ApJ, 508, 123

Förster Schreiber, N. M., Genzel, R., Lutz, D., Kunze, D., & Sternberg, A. 2001, ApJ, 552, 544

Franceschini et al. 2002, ApJ, 568, 470

Genzel, R., et al. 1998, ApJ, 498, 579

Genzel, R. & Cesarsky, C.J. 2000, ARA&A, 38, 761

Gruppioni et al. 2002, MNRAS, 335, 831

Houck, J. R., et al. 2004, ApJS, 154, 18

Houck, J. R., et al. 2005, ApJL, in press

Kim, D.-C. & Sanders, D.B. 1998, ApJS, 508, 627

Lacy, M. et al. 2005, ApJ, in press

Laurent, O., Mirabel, I. F., Charmandaris, V., Gallais, P., Madden, S. C., Sauvage, M., Vigroux, L., & Cesarsky, C. 2000, A&A, 359, 887

Lutz, D., Yan, L. et al. ApJ, 2005, in prep.

Lutz, D., Spoon, H. W. W., Rigopoulou, D., Moorwood, A. F. M., & Genzel, R. 1998, ApJ, 505, L103

Madau, P., Ferguson, H. C., Dickinson, M. E., Giavalisco, M., Steidel, C. C., & Fruchter, A. 1996, MNRAS, 283, 1388

Marleau, F. R., et al. 2004, ApJS, 154, 66

Papovich, C., et al. 2004, ApJS, 154, 70

Puget,J.-L.;Abergel, A.; Bernard,J.-P. et al. 1996, A&A, 308L, 5

Rigopoulou,D.;Spoon,H.W.W.;Genzel,R.;Lutz,D.;Moorwood,A.F.M.;Tran,Q.D. 1999, AJ, 118, 2625

Serjeant et al. 2000, MNRAS, 317, 29

Smail, I.; Ivison,R.J.;Blain,A.W. 1997, ApJL, 490, 5

Soifer, B. T., Sanders, D. B., Madore, B. F., Neugebauer, G., Danielson, G. E., Elias, J. H., Lonsdale, C. J., & Rice, W. L. 1987, ApJ, 320, 238

Spoon, H.W.W. et al. 2004, ApJS, 154, 184

Spoon, H. W. W., Moorwood, A. F. M., Lutz, D., Tielens, A. G. G. M., Siebenmorgen, R., & Keane, J. V. 2004, A&A, 414, 873

Tran, Q. D., et al. 2001, ApJ, 552, 527

Vermeij, R., & van der Hulst, J. M. 2002, A&A, 391, 1081

Voit, G. M. 1992, ApJ, 399, 495

Werner, M. W., et al. 2004, ApJS, 154, 1

Yan, Lin et al. 2004, ApJS, 154, 60

This preprint was prepared with the AAS LaTeX macros v5.2.

Table 1. IRS Low Resolution Spectroscopy Observation Log

ID	RA (J2000)	DEC (J2000)	$f(24\mu m)$ mJy	$f(8\mu m)$ μJy	R[a] mag	SL 1st seconds	LL 2nd seconds	LL 1st seconds
IRS1	17:18:44.378	+59:20:0.53	4.1	428	22.5	$1 \times 2 \times 240$	$2 \times 2 \times 120$	$3 \times 2 \times 120$
IRS2	17:15:38.182	+59:25:40.12	2.97	253	>25.5	$1 \times 2 \times 240$	$2 \times 2 \times 120$	$3 \times 2 \times 120$
IRS4	17:12:15.439	+58:52:27.88	2.3	261	23.0	$1 \times 2 \times 240$	$2 \times 2 \times 120$	$3 \times 2 \times 120$
IRS6	17:18:48.802	+58:56:56.83	2.03	95.5	24.7	···	$2 \times 2 \times 120$	$3 \times 2 \times 120$
IRS8	17:15:36.336	+59:36:14.76	1.34	<20	>25.5	···	$6 \times 2 \times 120$	$8 \times 2 \times 120$
IRS9	17:13:50.001	+58:56:56.83	1.28	93.5	>25.5	···	$6 \times 2 \times 120$	$8 \times 2 \times 120$
IRS10	17:21:24.581	+59:20:29.51	1.06	28	>25.5	···	$6 \times 2 \times 120$	$8 \times 2 \times 120$
IRS11	17:14:39.570	+58:56:32.10	0.96	56	23.5	···	$6 \times 2 \times 120$	$8 \times 2 \times 120$

[a] R band magnitude is in Vega system. The 3σ limit within an aperture of $3''$ in diameter is 25.5mag.

Table 2. Redshifts and spectral line measurements

ID	z	L_{ir}	$6.2\mu m$	$7.7\mu m$	$8.6\mu m$	$11.2\mu m$	$\tau_{9.7\mu m}$
IRS1	2.1 ± 0.1	3.2×10^{13}	···	$< 0.5(1.0)$[a]	···	···	1.77
IRS2	2.34 ± 0.06	4.3×10^{13}	3.7(3)	3.2(4.7)	1.3(3.8)	···	0.73
IRS6	2.4 ± 0.1	1.3×10^{13}	1.3(1.5)[b]	1(2.0)	···	···	1.43
IRS8	2.6 ± 0.2	2×10^{13}	···	$< 0.3(1.0)$	···	···	1.7
IRS9	1.83 ± 0.03	1.8×10^{13}	4.0(7.7)	5.2(6.6)[b]	2.7(4.4)	3.0(13.1)	1.2
IRS11	1.8 ± 0.15	5.8×10^{12}	···	1.7(2.5)	1.3(2)	···	>3

[a]For PAH feature, we listed two numbers – the first number is the observed line flux in unit of 10^{-15}ergs/s/cm^2, and the second number in the parenthesis is the signal-to-noise (S/N) ratio of the flux. For the sources (IRS2 and IRS8) without detectable PAH features, we listed the 1σ flux limit for 7.7μm feature only.

[b]The 6.2μm for IRS6 and the 7.7μm measurements for IRS9 are highly uncertain because the lines are at the edges of the two orders in the long-low module.

Table 3. Comparison with local ULIRGs

ID	z	L_{IR}[a] $L_\odot$	$\frac{L_{6.2\mu}}{L_{IR}}$	$\frac{L_{7.7\mu}}{L_{IR}}$	$\frac{L_{11.2\mu}}{L_{IR}}$	$EW^{rest}_{6.2\mu}$[b] μm	$EW^{rest}_{7.7\mu}$ μm	$EW^{rest}_{11.2\mu}$ μm	$\tau_{9.7\mu}$[c]
IRS2	2.34	4.3×10^{13}	1.1e-3	1e-3	···	0.08	0.13	···	0.73
IRS9	1.83	1.8×10^{13}	1.3e-3	2.2e-3[d]	1.2e-3	0.24	0.3	0.35	1.2
F00183-7111	0.327	7×10^{12}	<3.7e-4	···	4.4e-4	<0.011	···	0.182[d]	5
Mrk1014	0.1631	3.2×10^{12}	6.5e-5	1.5e-4	2.1e-5	0.048	0.022	0.017	0
UGC5101	0.0394	8.7×10^{11}	1.9e-3	5.5e-3	1.0e-3	0.248	0.553	0.273	2
NGC7714	0.0093	5.6×10^{10}	3.9e-3	7.9e-3	1.8e-3	0.50	0.70	0.17	0

[a]The total bolometric luminosity L_{IR} is for $3 - 1000\mu$m, and the unit is in $L_\odot$.

[b]the rest-frame equivalent width is in micron.

[c]Here $\tau_{9.7\mu}$ is computed from the minimum of the 9.7μm absorption, without fully integrating over the line. This value should be the lower limit.

[d]The data for the local galaxies in this table are from Spoon et al. (2004), Brandl et al. (2004), Armus et al. (2004). The rest-frame equivalent widths for F00183-7111 is from the private communication with H. Spoon (2004).